Conductivity in Carbon Nanotubes with Aharonov-Bohm Flux

Takeshi NAKANISHI and Tsuneya ANDO[1]

National Institute of Advanced Industrial Science and Technology
1 Umezono, Tsukuba 305-8568, Japan
and CREST, JST
4-1-8 Hon-machi, Kawaguchi, Saitama 332-0012 Japan

[1]*Department of Physics, Tokyo Institute of Technology*
2–12–1 Ookayama, Meguro-ku, Tokyo 152-8551, Japan

The Boltzmann conductivity is calculated for carbon nanotubes in the presence of an Aharonov-Bohm magnetic flux. Effects of impurity scattering are considered at low temperatures and those of electron-phonon scattering are considered at room temperature. Effects of strains and curvature manifest themselves as a prominent conductivity peak as a function of the flux. The appearance of the peak corresponds to the absence of backscattering in metallic linear bands.

Keywords: Aharonov-Bohm effect, Boltzmann conductivity, graphite, carbon nanotube, fullerene tube, effective-mass theory

§1. Introduction

Carbon nanotubes are novel quantum wires consisting of rolled graphite sheets.[1)] Single-wall nanotubes can be synthesized in structures ~ 1 nm in diameter and millimeters long.[2−4)] Their cylindrical shape leads to a strong Aharonov–Bohm (AB) effect in the band structure due to a magnetic field parallel to the axis.[5,6)] The purpose of this paper is to study conductivity in the presence of AB flux.

The electronic states change from metallic to semiconducting depending on the tubular circumferential vector characterizing a nanotube. The characteristic properties were predicted by calculations in tight-binding models[7−16)] and also in a $\boldsymbol{k}\cdot\boldsymbol{p}$ scheme or an effective-mass approximation.[17,18)] The AB effect on the band gap in nanotubes was theoretically predicted in the effective-mass approximation.[5,6,19,20)] Recently, splitting of optical absorption and emission peaks due to the AB effect was observed.[21)] A shift in the gate voltage corresponding to the conductance peak was also observed in Fabry-Perot interference regime and attributed to the AB effect.[22)]

Metallic nanotubes are known as a ballistic conductor due to the absence of backward scattering as long as the potential range of scatterers is not smaller than the lattice constant of two-dimensional graphite.[23−25)] When several bands are occupied, a perfectly conducting channel transmitting through the system without being scattered back is present.[26)] These intriguing features are due to the existence of a special symmetry present in the Schrödinger equation in the lowest-order $\boldsymbol{k}\cdot\boldsymbol{p}$ equation. The absence of backscattering is robust, but the perfect channel is fragile against various symmetry breaking effects such as a magnetic field and flux,[27)] short-range scatterers,[28)] and trigonal warping of the bands appearing in higher-order $\boldsymbol{k}\cdot\boldsymbol{p}$ terms.[29)] Metallic nanotubes are almost ballistic with a mean free path exceeding 1 μm even at room temperature.[30,31)] A lattice vacancy with strong and short-range potential causes an interesting conductance quantization.[32−37)]

Mechanical deformation is known to modify the band gap.[38,39)] In fact, the presence of a lattice distortion can be incorporated in the $\boldsymbol{k}\cdot\boldsymbol{p}$ scheme as an effective flux.[20,31,40−42)] It is also shown in the $\boldsymbol{k}\cdot\boldsymbol{p}$ scheme that the nonzero curvature causes an effective flux.[20,40,43)] Recent experiments on the conductance in metallic nanotubes are understood by taking a small gap induced by an effective flux into account.[22,44)] Nanotubes millimeters long synthesized recently by a water-assisted technique is likely to show a diffusive behavior.[4)]

In this paper, we shall calculate the Boltzmann conductivity in the $\boldsymbol{k}\cdot\boldsymbol{p}$ scheme and explore effects of AB flux on transport properties of nanotubes in the diffusive region. In §2, the $\boldsymbol{k}\cdot\boldsymbol{p}$ scheme is reviewed very briefly. Some examples of explicit results of the conductivity in the presence of flux are presented in §3 for impurity scatterings and in §4 for the electron-phonon scattering, demonstrating a possibility to directly determine a small gap present in metallic nanotubes experimentally. The results are discussed in §5 and summarized in §6.

§2. Effective-Mass Approximation

2.1 Energy bands and wave functions

The structure of a two-dimensional graphite is shown in Fig. 1 together with the first Brillouin zone and coordinate systems to be used in the following. In a two-dimensional graphite, two bands having approximately a linear dispersion cross the Fermi level (chosen at $\varepsilon = 0$) at K and K' points of the first Brillouin zone. Electronic states of the π-bands near a K point are described by the $\boldsymbol{k}\cdot\boldsymbol{p}$ equation:[17,20,45)]

$$\gamma(\sigma_x\hat{k}_x + \sigma_y\hat{k}_y)\boldsymbol{F}(\boldsymbol{r}) = \varepsilon\boldsymbol{F}(\boldsymbol{r}), \tag{2.1}$$

where γ is a band parameter, σ_x and σ_y are the Pauli spin matrices, and $\hat{\boldsymbol{k}} = (\hat{k}_x, \hat{k}_y) = -\mathrm{i}\boldsymbol{\nabla}$ is a wave-vector operator. Two components of the wave function $\boldsymbol{F}(\boldsymbol{r})$ correspond to the amplitude at A and B sites in a unit cell.

The structure of a nanotube is specified by a chiral vector $\boldsymbol{L}$ corresponding to the circumference as shown in

Fig. 1. It is written as

$$\boldsymbol{L} = n_a\boldsymbol{a}+n_b\boldsymbol{b}, \tag{2.2}$$

in terms of two integers n_a and n_b, where $\boldsymbol{a}$ and $\boldsymbol{b}$ are the primitive translation vectors of a graphite sheet. In the following we shall choose the x axis in the circumference direction and the y axis in the axis direction, i.e., $\boldsymbol{L} = (L, 0)$, where L is the circumference. The angle η between $\boldsymbol{L}$ and the horizontal axis is called the chiral angle. Electronic states of a nanotube with a sufficiently large diameter are obtained by imposing the boundary conditions around the circumference direction:

$$\boldsymbol{F}(\boldsymbol{r}+\boldsymbol{L})=\boldsymbol{F}(\boldsymbol{r})\exp(2\pi\mathrm{i}\Phi), \tag{2.3}$$

where $\Phi=-\nu/3$ with integer $\nu=0$ or ±1 determined by

$$n_a+n_b = 3M+\nu, \tag{2.4}$$

with integer M. Metallic and semiconducting nanotubes correspond to $\nu=0$ and ±1, respectively.

A nonzero curvature causes a shift in the origin of $\hat{k}_x$ and $\hat{k}_y$ in the $\boldsymbol{k}\cdot\boldsymbol{p}$ Hamiltonian. The shift in the y direction is irrelevant and that in the x direction can be replaced by an effective flux φ_s. The flux was estimated as[20,43]

$$\varphi_s = \frac{2\pi}{4\sqrt{3}}\frac{a}{L}p\cos 3\eta, \tag{2.5}$$

with a being the lattice constant of the two-dimensional graphite, $p=1-(3/8)\gamma'/\gamma$, $\gamma=-(\sqrt{3}/2)V_{pp}^{\pi}a$, and $\gamma'=-(\sqrt{3}/2)(V_{pp}^{\sigma}-V_{pp}^{\pi})a$, where V_{pp}^{π} ($=-\gamma_0$) and V_{pp}^{σ} are the conventional tight-binding parameters for neighboring p orbitals.[43] The curvature effect is largest in zigzag nanotubes with $\eta=0$ and absent in armchair nanotubes with $\eta=\pi/6$.

The presence of a lattice distortion $\boldsymbol{u}=(u_x,u_y,u_z)$ causes also an effective flux. It is estimated as[31]

$$\varphi_s = \frac{Lg_2}{2\pi\gamma}[(u_{xx}-u_{yy})\cos 3\eta-2u_{xy}\sin 3\eta], \tag{2.6}$$

where $u_{\mu\nu}$ ($\mu,\nu=x,y$) denotes the lattice strain given by

$$u_{xx}=\frac{\partial u_x}{\partial x}+\frac{2\pi u_z}{L},\quad u_{yy}=\frac{\partial u_y}{\partial y},\quad 2u_{xy}=\frac{\partial u_x}{\partial y}+\frac{\partial u_y}{\partial x}, \tag{2.7}$$

and g_2 is the electron-phonon interaction energy given by $g_2=(\alpha/2)\gamma_0$ with $\alpha\sim1$, where $\gamma=\sqrt{3}a\gamma_0/2$.[31,42] This shows that twist and stretch deformation give rise to nonzero flux in armchair $\eta=\pi/6$ and zigzag $\eta=0$ nanotubes, respectively.

In the presence of such flux φ_s due to finite curvature and strain, we have $\Phi=\varphi_e$ with

$$\varphi_e = -\frac{\nu}{3}+\varphi_s. \tag{2.8}$$

In the presence of flux ϕ due to a magnetic field parallel to the axis, further, we have

$$\Phi = \varphi+\varphi_e, \tag{2.9}$$

where $\varphi=\phi/\phi_0$ with the magnetic flux quantum $\phi_0=ch/e$. An effective flux, defined by

$$\phi_e = \varphi_e\phi_0, \tag{2.10}$$

is used also in the following.

The energy bands are specified by $s=\pm1$, integer n corresponding to the discrete wave vector along the circumference direction, and the wave vector k in the axis direction, where $s=+1$ and -1 denote the conduction and valence bands, respectively. The wave function for a band associated with the K point is written as

$$\boldsymbol{F}^{\mathrm{K}} = \frac{1}{\sqrt{2AL}}\begin{pmatrix} b_{\varphi+\varphi_e}(n,k)\\ s\end{pmatrix}\exp\left[\mathrm{i}\kappa_{\varphi+\varphi_e}(n)x+\mathrm{i}ky\right], \tag{2.11}$$

where A is the tube length,

$$\kappa_{\varphi+\varphi_e}(n) = \frac{2\pi}{L}(n+\varphi+\varphi_e), \tag{2.12}$$

and

$$b_{\varphi+\varphi_e}(n,k) = \frac{\kappa_{\varphi+\varphi_e}(n)-\mathrm{i}k}{\sqrt{\kappa_{\varphi+\varphi_e}(n)^2+k^2}}. \tag{2.13}$$

The corresponding energy is given by

$$\epsilon^s_{\varphi+\varphi_e}(n,k) = s\gamma\sqrt{\kappa_{\varphi+\varphi_e}(n)^2+k^2}. \tag{2.14}$$

The energy bands and wave functions for the K' point are obtained by replacing $\hat{k}_y$ by $-\hat{k}_y$ and in the boundary conditions φ_e by $-\varphi_e$. Correspondingly, we have $\kappa'=\kappa_{\varphi-\varphi_e}(n)$ and $b'=b_{\varphi-\varphi_e}(n,k)^*$.

Figure 2 shows an example of the energy dispersion of the band $n=0$ near the Fermi energy for small φ_e. In the absence of magnetic flux φ, as shown by dotted lines, the energy dispersions are the same between the K and K' points with gap $2|\varphi_e|(2\pi\gamma/L)$. When $\varphi_e>0$, the gap diminishes at the K' point by applying φ, while it increases at the K point, as shown by solid lines. The Fermi wave-number in the axis direction is denoted by k_0 for the K point and k_0' for the K' point, with

$$\begin{aligned} k_0 &= \sqrt{(\varepsilon/\gamma)^2-\kappa^2_{\varphi+\varphi_e}},\\ k_0' &= \sqrt{(\varepsilon/\gamma)^2-\kappa^2_{\varphi-\varphi_e}},\end{aligned} \tag{2.15}$$

for the Fermi energy ε, where

$$\kappa_{\varphi\pm\varphi_e} \equiv \kappa_{\varphi\pm\varphi_e}(0), \tag{2.16}$$

for simplicity. When the electron concentration is sufficiently small, the K point or the K' point is depopulated by electrons for sufficiently large magnetic flux φ. At $\varphi=\varphi_e$, the dispersion becomes completely linear at the K' point. The same thing happens for the K point at $\varphi=-\varphi_e$.

The conductivity is evaluated under two different conditions, fixed energy and electron density. The latter is expected to be more appropriate for long nanotubes exhibiting diffusive conduction. The electron density is characterized by the average Fermi wave number k_+ defined by

$$k_+ = \frac{1}{2}(k_0+k_0'). \tag{2.17}$$

2.2 Effective potential of impurity

Most of scatterers including charged centers are

expected to be characterized by a potential with range larger than the lattice constant a. For such scatterers, the Hamiltonian is given by a diagonal matrix for both K and K' points, and matrix elements between K and K' points are safely neglected.[23] These scatterers will be called *long-range* although their potential range can be comparable to the lattice constant and therefore can actually be much shorter than the electron wavelength typically of the order of the nanotube circumference. In the following, we shall confine ourselves to the case that the potential range of *long-range* scatterers is sufficiently smaller than the circumference. In this case we can replace the potential of each scatterer by a delta function with strength u_L.

When the potential range becomes shorter than the lattice constant, the potential for A and B sub-lattice points in a unit cell can be different and matrix elements between K and K' points can no longer be neglected. As such scatterers, we shall consider those with potential range much smaller than the lattice constant and strength u_S, giving rise to the same amplitude for scattering within the K and K' points and for scattering between the K and K' points. These scatterers are called *short-range* in the following.

In the lowest Born approximation the scattering strength for long- and short-range scatterers is characterized by the dimensionless quantity W_L and W_S, respectively, with

$$W_L = \frac{n_L\langle|u_L|^2\rangle}{4\pi\gamma^2}, \quad W_S = \frac{n_S\langle|u_S|^2\rangle}{4\pi\gamma^2}, \tag{2.18}$$

where n_L and n_S are the concentration of long- and short-range scatterers in a unit area, respectively.[28] In the following, we shall fix the total strength W with

$$W = W_L + W_S, \tag{2.19}$$

and vary the parameter δ defined by

$$\delta = \frac{W_S}{W}, \tag{2.20}$$

in order to see effects of short-range scatterers.[28]

2.3 Effective potential for phonon

The electron-phonon interaction is considered in a continuum model for long-wavelength acoustic phonons. An effective Hamiltonian for the electron-phonon interaction for the K point is given by[31]

$$\mathcal{H}_{\text{el-ph}} = \begin{pmatrix} V_1 & V_2 \\ V_2^* & V_1 \end{pmatrix}, \tag{2.21}$$

with

$$\begin{aligned} V_1 &= g_1(u_{xx}+u_{yy}), \\ V_2 &= g_2 \mathrm{e}^{3\mathrm{i}\eta}(u_{xx}-u_{yy}+2\mathrm{i}u_{xy}), \end{aligned} \tag{2.22}$$

where the strain tensor is defined in eq. (2.7). The Hamiltonian for the K' point is obtained by replacing V_2 with $-V_2^*$ and V_2^* with $-V_2$. The diagonal term represents coupling through the deformation potential g_1 and the off-diagonal coupling g_2 through the bond-length change. It has been shown that $g_1 \gg g_2$.[31] Note that eq. (2.6) is derived easily from eq. (2.21).

Phonons contributing to the electron scattering are described well by the potential-energy functional

$$U[\boldsymbol{u}] = \int \mathrm{d}x\mathrm{d}y \frac{1}{2}\{B(u_{xx}+u_{yy})^2+\mu[(u_{xx}-u_{yy})^2+4u_{xy}^2]\}, \tag{2.23}$$

where B and μ are the bulk and shear modulus, respectively. An elastic scattering approximation is employed, because the phonon velocity is much slower than the electron. Further, a high-temperature approximation is used for the phonon distribution function. Then, the relaxation time due to electron-phonon scattering becomes independent of the chirality η.[31]

2.4 Boltzmann conductivity

In this study, we calculate the Boltzmann conductivity

$$\sigma = \frac{e^2}{\pi\hbar}\sum_m \Lambda_m(\varepsilon), \tag{2.24}$$

where $\Lambda_m(\varepsilon)$ is the mean free path.[27,46] It satisfies the transport equation

$$\sum_{m'}(K_{m-m'+}-K_{m+m'+})\Lambda_{m'}(\varepsilon) = 1, \tag{2.25}$$

where m and m' denote the bands crossing the energy ε, and $+(-)$ the wave vector corresponding to the positive (negative) velocity in the y direction. The kernel for the transport equation is given by

$$K_{\nu\mu} = \frac{A\langle|V_{\nu\mu}|^2\rangle}{\hbar^2|v_\nu v_\mu|}, \tag{2.26}$$

for $\nu \neq \mu$, where v_μ is the velocity of mode $\mu \equiv (m\pm)$ and $\langle\cdots\rangle$ denotes an average over impurities or a thermal average. The diagonal elements are defined by

$$K_{\mu\mu} = -\sum_{\nu\neq\mu} K_{\nu\mu}. \tag{2.27}$$

§3. Impurity Scattering

3.1 Conductivity

When a magnetic flux is present, the occupation of the bands varies and some bands can be depopulated by electrons completely. First, we shall consider the case that such depopulation does not occur and the lowest conduction band is occupied by electrons for both K and K' points. In this case the Fermi energy ε is related to k_+ given by eq. (2.17) through

$$\varepsilon = \frac{2\pi\gamma}{L}\sqrt{\Big[1+\Big(\frac{2\pi\varphi_e}{k_+L}\Big)^2\Big]\varphi^2+\varphi_e^2+\Big(\frac{k_+L}{2\pi}\Big)^2}. \tag{3.1}$$

This shows that ε increases with the magnetic flux φ.

The conductivity is given by

$$\sigma(\varphi) = \frac{e^2}{\pi\hbar}(\Lambda^K+\Lambda^{K'}), \tag{3.2}$$

where Λ^K and $\Lambda^{K'}$ are the mean free path for the K and

K' points. For the K point, we have

$$\begin{aligned}\frac{1}{\Lambda^K} &= \frac{1}{\Lambda_L^K}+\frac{1}{\Lambda_S^K},\\ \frac{1}{\Lambda_L^K} &= \frac{2\pi W(1-\delta)}{L}\frac{\kappa_{\varphi+\varphi_e}^2}{k_0^2},\\ \frac{1}{\Lambda_S^K} &= \frac{2\pi W\delta}{L}\Big(1+\frac{\kappa_{\varphi+\varphi_e}^2}{k_0^2}\Big)^{1/2}\\ &\quad\times\Big[\Big(1+\frac{\kappa_{\varphi+\varphi_e}^2}{k_0^2}\Big)^{1/2}+\Big(1+\frac{\kappa_{\varphi-\varphi_e}^2}{{k_0'}^2}\Big)^{1/2}\Big],\end{aligned} \tag{3.3}$$

where Λ_L^K and Λ_S^K are contributions of long- and short-range scatterers, respectively. The results for the K' point, $\Lambda^{K'}$, $\Lambda_L^{K'}$, and $\Lambda_S^{K'}$, are given by exchanging k_0 and k_0' and replacing φ_e with $-\varphi_e$.

The absence of backward scattering[23] corresponds to the divergence of Λ_L^K at $\varphi=-\varphi_e$ and $\Lambda_L^{K'}$ at $\varphi=+\varphi_e$, giving rise to infinitely large conductivity in the absence of short-range scatterers, i.e., $\delta=0$. At these values of the flux, therefore, the mean free path and the conductivity of the corresponding point are determined by scattering by short-range scatterers.

3.2 Metallic nanotubes

In metallic nanotubes, the effective flux is very small, i.e, $|\varphi_e|\ll 1$, and therefore the condition $\varphi=+\varphi_e$ or $\varphi=-\varphi_e$ can be reached easily using a conventional magnet. In the vicinity of $\varphi=-\varphi_e$, for example, the mean free path for the K point is written as

$$\frac{1}{\Lambda^K}=\frac{2\pi W}{L}\Big(\frac{2\pi}{Lk_0}\Big)^2(1-\delta)[(\varphi+\varphi_e)^2+\Delta\varphi^2], \tag{3.4}$$

with

$$\Delta\varphi=\sqrt{\frac{\delta}{1-\delta}}\frac{Lk_0}{2\pi}\Big(1+\Big[1+4\varphi_e^2\Big(\frac{2\pi}{Lk_0'}\Big)^2\Big]^{1/2}\Big)^{1/2}. \tag{3.5}$$

Therefore, the mean free path exhibits a Lorentzian-like peak at $\varphi=-\varphi_e$ with width $\Delta\varphi$. The condition that $\sigma(\varphi)$ has actually a peak can be obtained approximately by the condition $\sigma(\varphi_e)>\sigma(0)$ as $\Delta\varphi<\sqrt{2}|\varphi_e|$. For $Lk_+/2\pi\gg|\varphi_e|$, for example, we have $k_0\approx k_0'\approx k_+$ and therefore the condition for the peak appearance becomes $\sqrt{\delta/(1-\delta)}(Lk_+/2\pi)<|\varphi_e|$.

When $\sqrt{\delta/(1-\delta)}(Lk_+/2\pi)\gg|\varphi_e|$, the contribution of long-range scatterers can be neglected safely and the conductivity is given by

$$\sigma(\varphi)=\frac{e^2L}{2\pi^2\hbar W\delta}\Big(1+\frac{\kappa_{\varphi+\varphi_e}^2}{k_0^2}\Big)^{-1/2}\Big(1+\frac{\kappa_{\varphi-\varphi_e}^2}{k_0^2}\Big)^{-1/2}. \tag{3.6}$$

This does not exhibit any peak structure at $\varphi\sim\pm\varphi_e$, but rather decreases with the increase of φ and approaches the value independent of φ and φ_e,

$$\sigma(\varphi)\to\frac{e^2L}{2\pi^2\hbar W\delta}. \tag{3.7}$$

for $Lk_+/2\pi\gg|\varphi_e|$.

Figure 3 shows some examples of the conductivity for $\delta=0.01$ as a function of φ/φ_e with the fixed electron density. A prominent peak appears for the small electron density k_+. Note that, results for a fixed Fermi energy are similar to those for the fixed density in this region of the electron density.

Figure 4 shows the conductivity for several values of δ at $(k_+L/2\pi)/\varphi_e=5$. For $\delta=0$ the conductivity diverges at $\varphi=\varphi_e$. For nonzero δ, the peak appears and its height decreases with the increase of δ. The peak disappears around $\delta=0.04$, in agreement with the condition obtained above.

3.3 Semiconducting nanotubes

In semiconducting nanotubes, the effective flux is given by $\varphi_e\approx\pm1/3$ ($\pm$ depending on the structure). It is almost impossible to reach this amount of the flux using conventional magnets for which $\varphi\ll1$. We can discuss only whether the flux tends to increase or decrease the conductivity. The first derivative $\mathrm{d}\sigma/\mathrm{d}\varphi$ at $\varphi=0$ vanishes identically because $\mathrm{d}\Lambda_K/\mathrm{d}\varphi$ and $\mathrm{d}\Lambda_{K'}/\mathrm{d}\varphi$ cancel each other, and therefore we have

$$\sigma(\varphi)=\sigma(0)+\frac{1}{2}\sigma''(0)\varphi^2+\dots. \tag{3.8}$$

When the electron concentration is not extremely large we have $Lk_+/2\pi\ll1/3$. In this case, we have

$$\sigma''(0)=\frac{4e^2}{\pi\hbar W}\frac{2\pi}{L}\frac{1-4\delta-\delta^2}{(1+\delta)^3}\frac{1}{k_+^2}, \tag{3.9}$$

for a fixed electron density. It is positive for $\delta<\sqrt{5}-2=0.236\dots$ and negative otherwise.

It is concluded, therefore, that a usual semiconducting nanotube exhibits a positive magnetoconductivity, its amount being strongly dependent on the electron concentration. Only dirty semiconducting nanotubes containing large amount of short-range scatterers exhibit a negative magnetoconductivity. The tendency that dominant long-range scatterers cause a positive magnetoconductivity, while short-range scatterers cause a negative magnetoconductivity, corresponds to the behavior of the peak structure in metallic nanotubes, discussed in the previous section.

3.4 Band depopulation

When the electron concentration is small and the band edge of K and K' points cross the Fermi level as a function of the flux, the conductivity exhibits a singular behavior depending strongly on whether the electron density or the Fermi level is fixed. Several examples of calculated Fermi energy are shown with the fixed electron densities as a function of the magnetic flux for $\varphi_e>0$ in Fig. 5. The band edges $\gamma|\kappa_{\varphi-\varphi_e}|$ and $\gamma|\kappa_{\varphi+\varphi_e}|$ are also shown by thin solid and dotted lines, respectively. Only the K' point is populated in the region between the solid and dotted thin lines, and both K and K' points are populated above the dotted thin lines. Near the band edges, the corresponding energy strongly depends on the magnetic flux.

The conductivity under the condition of a fixed energy and a fixed electron density are shown in Figs. 6 and 7, respectively. At a critical flux the conductivity vanishes due to the divergence in the scattering probability caused by the infinite density of states characteristic

of the one-dimensional system. Beyond this flux the K point is depopulated completely and electrons are only in the band associated with the K' point. Apart from this singular behavior, the conductivity has a general tendency to exhibit a peak at $\varphi=\varphi_e$ (also at $\varphi=-\varphi_e$).

§4. Electron-Phonon Scattering

In the presence of the electron-phonon interaction eq. (2.21), where the scattering is only within the K point or K' point, we have the conductivity

$$\sigma(\varphi) = \frac{e^2}{\pi\hbar}(\Lambda^K+\Lambda^{K'}), \tag{4.1}$$

with

$$\frac{1}{\Lambda^K} = \frac{2\pi}{L}\frac{k_BT}{\gamma^2}\Big[\frac{g_1^2}{B}\frac{\kappa_{\varphi+\varphi_e}^2}{k_0^2}+\frac{g_2^2}{\mu}\Big(1+\frac{\kappa_{\varphi+\varphi_e}^2}{k_0^2}\Big)\Big], \tag{4.2}$$

and $\Lambda_{K'}$ obtained by replacing $\kappa_{\varphi+\varphi_e}$ with $\kappa_{\varphi-\varphi_e}$ and k_0 with k_0'. When only a single valley is occupied, the conductivity is given by its contribution alone. For $\varphi=\varphi_e=0$, in particular, this expression is reduced to

$$\sigma_A=\frac{e^2}{h}\frac{2L\gamma^2\mu}{g_2^2k_BT}, \tag{4.3}$$

obtained previously.[31)]

Figure 8 shows the conductivity of a metallic nanotube as a function of the magnetic flux under the condition of a fixed electron density for $g_1/g_2=10$ and $B/\mu=3/\sqrt{2}$.[31)] A peak with height $\sim\sigma_A/2$ appears at $\varphi=\varphi_e$ when the electron density is low. With the increase of the electron density, the peak becomes less prominent and disappears around $(k_+L/2\pi)/(\phi_e/\phi_0)\sim 10$. This behavior is very similar to the case of the impurity scattering in Fig. 3 for $\delta=0.01$. The conductivity approaches σ_A for sufficiently large electron density. The figure contains also some results for a small electron density [$(k_+L/2\pi)/\varphi_e=1$, 0.5, and 0.25] for which the K or K' valley is depopulated with the increase of the flux. No singular behavior appears even in such a case.

In semiconducting nanotubes with $\varphi_e\approx\pm1/3$ and $k_+L/2\pi\ll1$, we have eq. (3.8) with

$$\sigma''(0)=\sigma_A\frac{2Bg_2^2}{Bg_2^2+\mu g_1^2}\Big(\frac{2\pi}{k_+L}\Big)^2. \tag{4.4}$$

Therefore, a semiconducting nanotube almost always exhibits a positive magnetoconductivity and its amount is strongly dependent on the electron concentration.

§5. Discussion

An effective flux due to the curvature of a nanotube (eq. (2.5)) is estimated as $\varphi_s\sim0.05\times p\cos3\eta$ for a typical nanotube with $L\sim5$ nm with a parameter $|p|<1$.[43)] This flux is the greatest in the zigzag tubes with $\eta=0$, followed by chiral tubes, and is nonexistent in the armchair tubes with $\eta=\pi/6$, as confirmed by an experiment with numerical simulations.[22)] An effective flux appears in the presence of uniaxial stress as well as a hydrostatic pressure because of eq. (2.6). The total effective flux can vary among different nanotubes although their structure is the same. The present calculation shows that the effective flux can be measured directly by a sharp peak as a function of the applied magnetic flux in metallic nanotubes. In fact, the flux can be as large as $\phi/\phi_0=5\times10^{-3}$ at 10 T for a typical nanotube with $L\sim5$ nm.

The sharpness of the conductivity peak as a function of the flux is sensitive to the electron density and the amount of short-range scatterers. The electron density may be controlled by a gate voltage and therefore a careful analysis of the gate-voltage dependence in the presence of a flux can give important information on dominant scatterers in metallic nanotubes.

At a room temperature, electron-phonon scattering constitutes the main origin of the resistivity, and the conductivity is likely to exhibit a peak structure as a function of an applied flux in metallic nanotubes. A careful analysis of possible gate-voltage dependence can reveal the relative strength of the electron-phonon interaction through a deformation potential and a bond-length change.

In metallic nanotubes with linear dispersion, effects of electron-electron interaction of a Tomonaga-Luttinger type[47–53)] can be important and may modify the flux dependence. The fact that the conductivity exhibits a sharp peak as a function of a magnetic flux is expected to be valid even if such interaction effects are considered.

Whether we have positive or negative magnetoconductivity in semiconducting nanotubes in the presence of a flux can depend on the change in the strength of screening effects. The static screening constant in the long-wavelength limit is determined by the density of states

$$\begin{aligned} D(\varphi) &= \frac{\hbar}{\gamma}\Big(1+\frac{\kappa_{\varphi+\varphi_e}^2}{k_0^2}\Big)^{1/2}+\frac{\hbar}{\gamma}\Big(1+\frac{\kappa_{\varphi-\varphi_e}^2}{{k_0'}^2}\Big)^{1/2} \\ &= D(0)+\frac{1}{2}D''(0)\varphi^2+\dots. \end{aligned} \tag{5.1}$$

For $\varphi_e\approx\pm1/3$ and $k_+L/2\pi\ll1$, we have

$$D''(0)\approx\frac{4}{27}\frac{\hbar}{\gamma}\Big(\frac{2\pi}{k_+L}\Big)^5, \tag{5.2}$$

under the condition of a fixed electron density. The second derivative is positive also under the condition of a fixed energy. Thus, the screening has a tendency to be enhanced due to flux. For the conductivity, however, screening for the wave number $2k_+$ is important. The logarithmic divergence of the screening function at $2k_+$ is known to be responsible to a power-law temperature dependence of the conductivity.[54,55)] This screening problem in the presence of flux is left for a future study.

§6. Conclusion

We have calculated the Boltzmann conductivity in carbon nanotubes in the presence of a magnetic flux in the $\boldsymbol{k}\cdot\boldsymbol{p}$ scheme. A gap induced by strain or curvature effects can be identified as a peak in the conductivity by applying an Aharonov-Bohm flux in metallic nanotubes. The peak corresponds to the absence of backscattering in metallic nanotubes with no effective flux. Various information on curvature and strain effects and the relative amount of short-range scatterers can be obtained by

careful measurement of the conductivity in the presence of the magnetic flux and by changing the electron density through a gate voltage. Semiconducting nanotubes exhibit a positive magnetoconductivity and its amount increases with the decrease of the electron concentration. Experiments along these lines are highly desired.

Acknowledgments

This work has been supported in part by a NAREGI nano-science project, by a 21st Century COE Program at Tokyo Tech "Nanometer-Scale Quantum Physics", and by Grant-in-Aid for Scientific Research from the Ministry of Education, Culture, Sports, Science and Technology, Japan.

References

1) S. Iijima: Nature (London) **354** (1991) 56.
2) S. Iijima and T. Ichihashi: Nature (London) **363** (1993) 603.
3) D. S. Bethune, C. H. Kiang, M. S. de Vries, G. Gorman, R. Savoy, J. Vazquez and R. Beyers: Nature (London) **363** (1993) 605.
4) K. Hata, D. N. Futaba, K. Mizuno, T. Namai, M. Yumura and S. Iijima: Science **306** (2004) 1362.
5) H. Ajiki and T. Ando: J. Phys. Soc. Jpn. **62** (1993) 2470; J. Phys. Soc. Jpn. **63** (1994) 4267 (Erratum).
6) H. Ajiki and T. Ando: Physica B **201** (1994) 349.
7) N. Hamada, S. Sawada and A. Oshiyama: Phys. Rev. Lett. **68** (1992) 1579.
8) J. W. Mintmire, B. I. Dunlap and C. T. White: Phys. Rev. Lett. **68** (1992) 631.
9) R. Saito, M. Fujita, G. Dresselhaus and M. S. Dresselhaus: Phys. Rev. B **46** (1992) 1804.
10) R. Saito, M. Fujita, G. Dresselhaus and M. S. Dresselhaus: Appl. Phys. Lett. **60** (1992) 2204.
11) M. S. Dresselhaus, G. Dresselhaus and R. Saito: Phys. Rev. B **45** (1992) 6234.
12) R. A. Jishi, M. S. Dresselhaus and G. Dresselhaus: Phys. Rev. B **47** (1993) 16671.
13) K. Tanaka, K. Okahara, M. Okada and T. Yamabe: Chem. Phys. Lett. **191** (1992) 469.
14) Y. D. Gao and W. C. Herndon: Mol. Phys. **77** (1992) 585.
15) D. H. Robertson, D. W. Brenner and J. W. Mintmire: Phys. Rev. B **45** (1992) 12592.
16) C. T. White, D. C. Robertson and J. W. Mintmire: Phys. Rev. B **47** (1993) 5485.
17) H. Ajiki and T. Ando: J. Phys. Soc. Jpn. **62** (1993) 1255.
18) H. Ajiki and T. Ando: Physica B **216** (1996) 358.
19) T. Ando: Semicond. Sci. & Technol. **15** (2000) R13.
20) T. Ando: J. Phys. Soc. Jpn. **74** (2005) 777.
21) S. Zaric, G. N. Ostojic, J. Kono, J. Shaver, V. C. Moore, M. S. Strano, R. H. Hauge, R. E. Smalley and X. Wei: Science **304** (2004) 1129.
22) J. Cao, Q. Wang, M. Rolandi and H. Dai: Phys. Rev. Lett. **93** (2004) 216803.
23) T. Ando and T. Nakanishi: J. Phys. Soc. Jpn. **67** (1998) 1704.
24) T. Ando, T. Nakanishi and R. Saito: J. Phys. Soc. Jpn. **67** (1998) 2857.
25) T. Nakanishi and T. Ando: J. Phys. Soc. Jpn. **68** (1999) 561.
26) T. Ando and H. Suzuura: J. Phys. Soc. Jpn. **71** (2002) 2753.
27) T. Ando: J. Phys. Soc. Jpn. **73** (2004) 1273.
28) T. Ando and K. Akimoto: J. Phys. Soc. Jpn. **73** (2004) 1895.
29) K. Akimoto and T. Ando: J. Phys. Soc. Jpn. **73** (2004) 2194.
30) H. Suzuura and T. Ando: Physica E **6** (2000) 864; Mol. Cryst. Liq. Cryst. **340** (2000) 731; *Proceedings of 25th International Conference on the Physics of Semiconductors*, edited by N. Miura and T. Ando (Springer, Berlin, 2001), p. 1525; *Nanonetwork Materials*, edited by S. Saito, T. Ando, Y. Iwasa, K. Kikuchi, M. Kobayashi and Y. Saito (American Institute of Physics, New York, 2001), p. 269.
31) H. Suzuura and T. Ando: Phys. Rev. B **65** (2002) 235412.
32) L. Chico, L. X. Benedict, S. G. Louie and M. L. Cohen: Phys. Rev. B **54** (1996) 2600; Phys. Rev. B **61** (2000) 10511 (Erratum).
33) M. Igami, T. Nakanishi and T. Ando: J. Phys. Soc. Jpn. **68** (1999) 716; *ibid* **68** (1999) 3146; Physica B **284-288** (2000) 1746; Mol. Cryst. Liq. Cryst. **340** (2000) 719.
34) T. Ando, T. Nakanishi and M. Igami: J. Phys. Soc. Jpn. **68** (1999) 3994.
35) T. Nakanishi, M. Igami and T. Ando: Physica E **6** (2000) 872.
36) H. J. Choi, J. -S. Ihm, S. G. Louie and M. L. Cohen: Phys. Rev. Lett. **84** (2000) 2917.
37) M. Igami, T. Nakanishi and T. Ando: J. Phys. Soc. Jpn. **70** (2001) 481.
38) L. Yang, M. P. Anantram, J. Han and J. P. Lu: Phys. Rev. B **60** (1999) 13874.
39) L. Yang and J. Han: Phys. Rev. Lett. **85** (2000) 154.
40) C. L. Kane and E. J. Mele: Phys. Rev. Lett. **78** (1997) 1932.
41) C. L. Kane, E. J. Mele, R. S. Lee, J. E. Fischer, P. Petit, H. Dai, A. Thess, R. E. Smalley, A. R. M. Verschueren, S. J. Tans and C. Dekker: Europhys. Lett. **41** (1998) 683.
42) T. Ando: J. Phys. Soc. Jpn. **73** (2004) 3351.
43) T. Ando: J. Phys. Soc. Jpn. **69** (2000) 1757.
44) P. Jarillo-Herrero, J. Kong, H. S. J. van der Zant, C. Dekker, L. P. Kouwenhoven and S. de Franceschi: Nature **434** (2005) 484.
45) J. C. Slonczewski and P. R. Weiss: Phys. Rev. **109** (1958) 272.
46) T. Seri and T. Ando: J. Phys. Soc. Jpn. **66** (1997) 169.
47) S. Tomonaga: Prog. Theor. Phys. **5** (1950) 544.
48) J. M. Luttinger: J. Math. Phys. **4** (1963) 1154.
49) L. Balents and M. P. A. Fisher: Phys. Rev. B **55** (1997) 11973.
50) Yu. A. Krotov, D. -H. Lee and S. G. Louie: Phys. Rev. Lett. **78** (1997) 4245.
51) C. Kane, L. Balents and M. P. A. Fisher: Phys. Rev. Lett. **79** (1997) 5086.
52) R. Egger and A. O. Gogolin: Eur. Phys. J. B **3** (1998) 281.
53) H. Yoshioka and A. A. Odintsov: Phys. Rev. Lett. **82** (1999) 374.
54) K. A. Matveev, D. Yue and L. I. Glazman: Phys.

Rev. Lett. **71** (1993) 3351.
55) A. Kawabata: J. Phys. Soc. Jpn. **63** (1994) 2047.

Figure Captions

Fig. 1 (a) Lattice structure of a two-dimensional graphite sheet. The coordinates (x', y') are fixed on the graphite sheet and (x, y) are chosen in such a way that x is along the circumference and y is along the axis. η is the chiral angle. (b) The first Brillouin zone and K and K' points. (c) The coordinates for the nanotube. An Aharonov-Bohm flux ϕ is applied in the axis direction of the nanotube.

Fig. 2 A schematic view of the bands near the Fermi energy. In the absence of a magnetic flux shown by dotted lines, the energy gaps of $4\pi\gamma|\varphi_e|/L$ are present at the K and K' point. As shown by solid lines, the band gap diminishes at the K' point and increases at the K point in the presence of magnetic flux ϕ for $\varphi_e > 0$. k_0 and k_0' are the Fermi wave-number measured from K and K' points, respectively.

Fig. 3 Calculated Boltzmann conductivity for several values of the electron density k_+, when electrons occupy the lowest conduction band of the K and K' points. The ratio of the short-range scatterers is chosen as $\delta = 0.01$.

Fig. 4 Boltzmann conductivity for several values of δ for the electron density $(k_+L/2\pi)/\varphi_e = 5$.

Fig. 5 The Fermi energy as a function of the magnetic flux $\varphi = \phi/\phi_0$ for several values of the electron density k_+ for $\varphi_e > 0$. The band edges are shown by thin lines, where solid and dotted lines are for K' and K point, respectively. Only the K' point is populated in the region between the solid and dotted thin lines and both K and K' points are populated above the dotted thin lines.

Fig. 6 Boltzmann conductivity with fixed Fermi energy at low concentrations.

Fig. 7 Boltzmann conductivity with fixed electron density at low concentrations.

Fig. 8 Calculated conductivity dominated by electron-phonon scattering as a function of the AB flux φ for several values of the fixed electron density. The phonon parameters are $g_1/g_2 = 10$ and $B/\mu = 3/\sqrt{2}$.

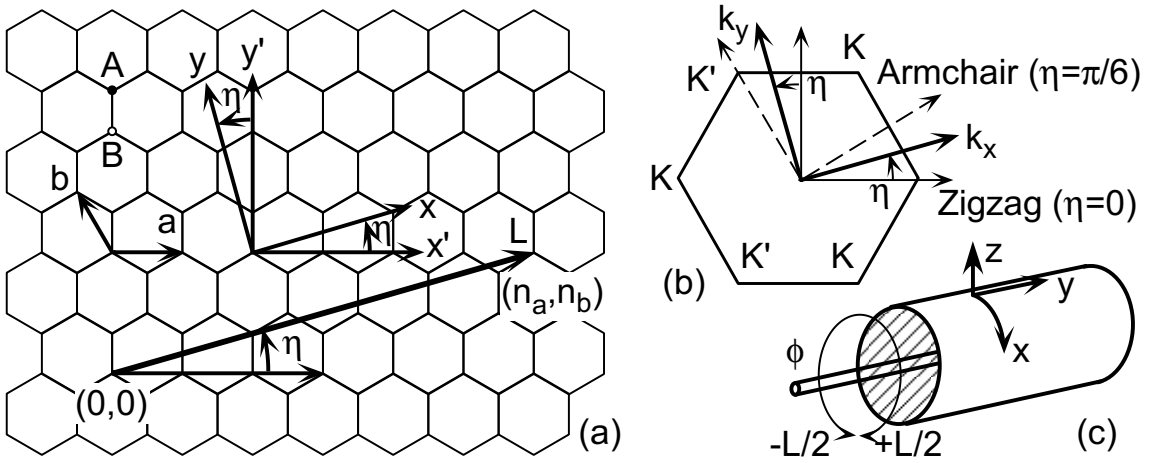

Fig. 1

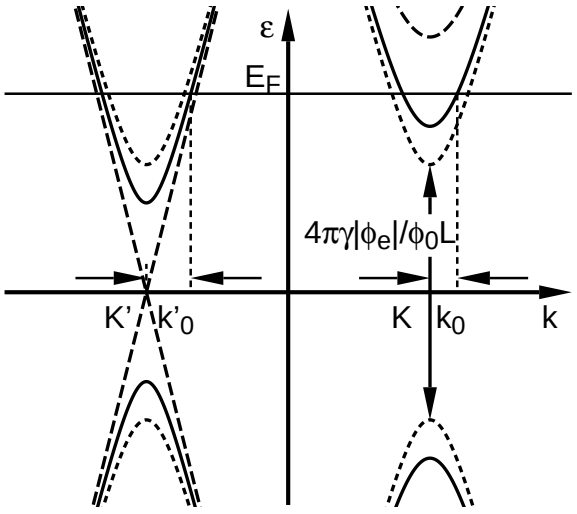

Fig. 2

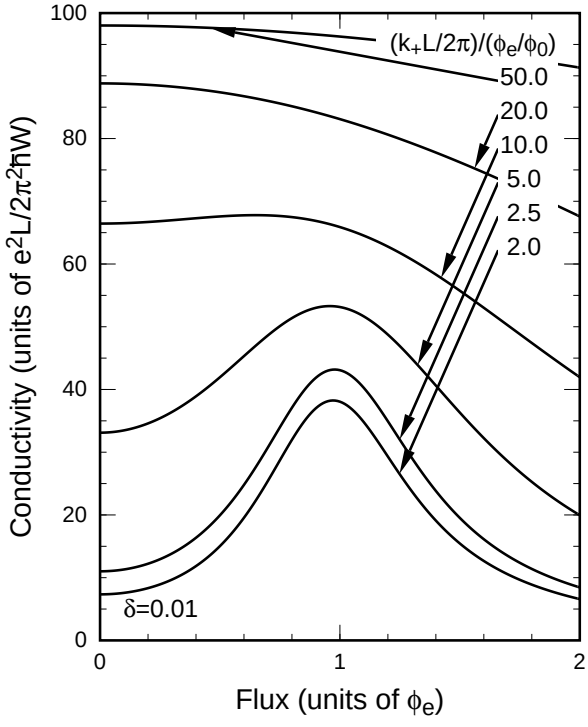

Fig. 3

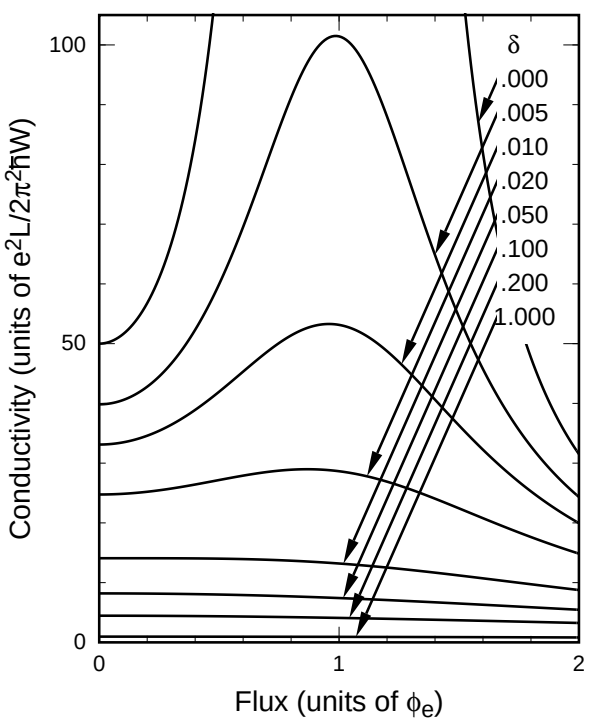

Fig. 4

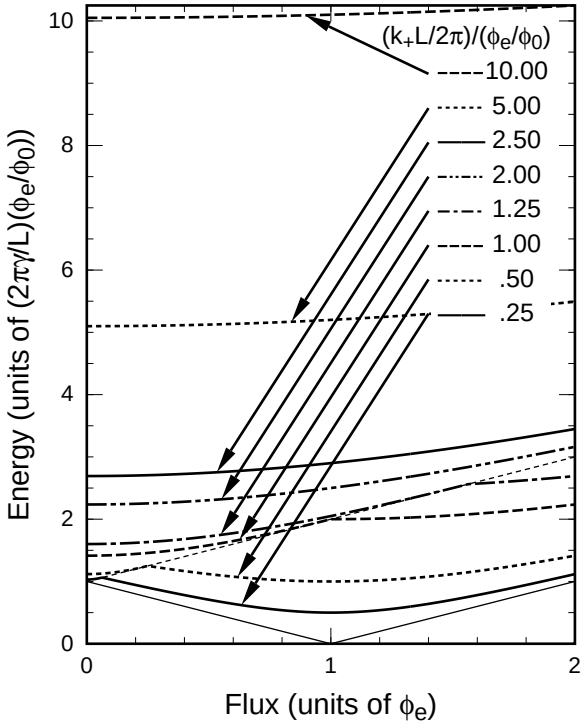

Fig. 5

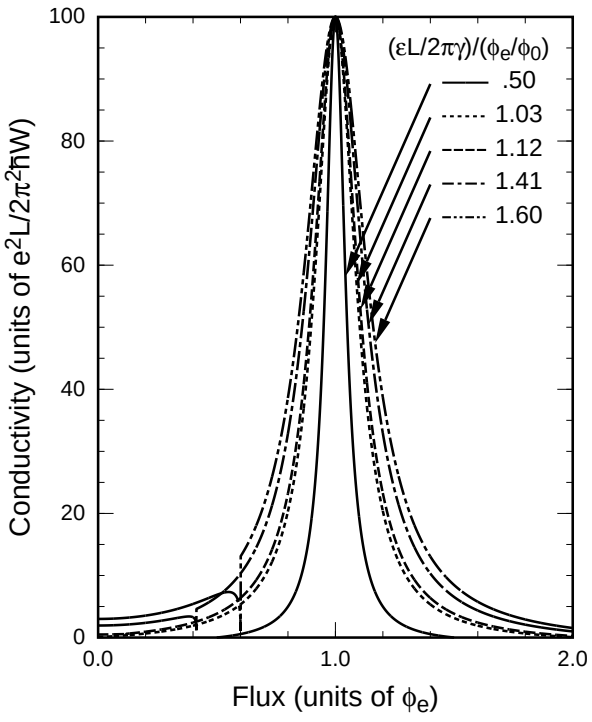

Fig. 6

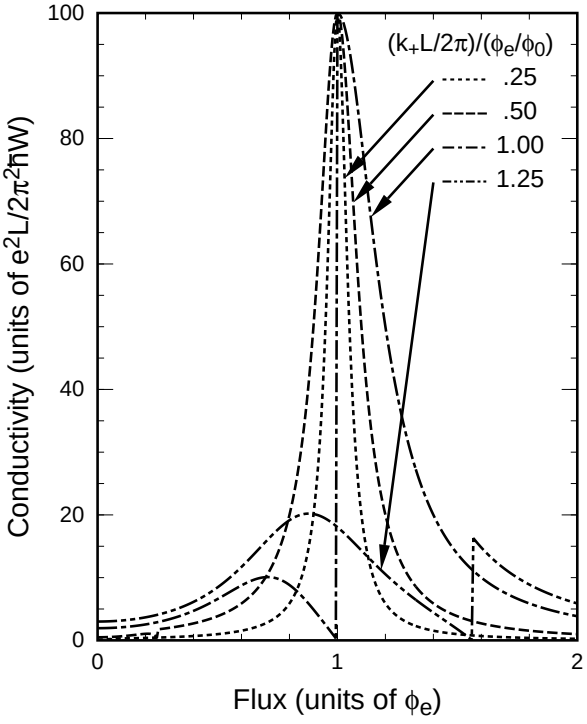

Fig. 7

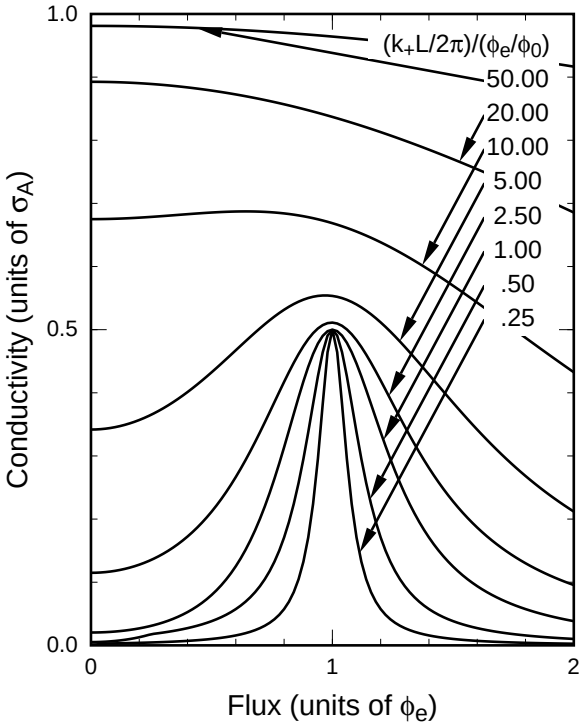
1.0
0.5
0.0
0
1
2
Conductivity (units of σ_A)
Flux (units of ϕ_e)
$(k_+L/2\pi)/(\phi_e/\phi_0)$
50.00
20.00
10.00
5.00
2.50
1.00
.50
.25

Fig. 8